

Using Super-Resolution Nanorulers to study the Capabilities of EM-CCD and sCMOS Cameras beyond the Diffraction Limit

Light microscopes enabling super-resolution imaging suffer from a standardized quantification method. We demonstrate the quantification of a super-resolution microscope by using standardized DNA origami samples with the help of two leading camera technologies (EM-CCD and sCMOS).

1. Overview

Recently, the Nobel Prize in chemistry was awarded to Stephan Hell, Eric Betzig and William E. Moerner for their groundbreaking improvements in optical and single molecule microscopy. Their fundamental work and innovative approaches made it possible to image structures smaller than the diffraction barrier of light (~200 nm), a limit which was first introduced by Ernst Abbe 1873. The development of novel types of microscopes, so called 'super-resolution' microscopes, enabled the visualization of biological processes on a molecular level and improved the insight in diverse fields of biomedicine such as neuroscience, morphogenesis or drug delivery, to name a few. Researchers developed a large number of methods to overcome the diffraction barrier based on spatiotemporal fluorescent switching.

In this paper, we performed a standard single molecule switching nanoscopy (SMSN) technique to demonstrate how two camera technologies (EM-CCD and sCMOS) can resolve the world's first standardized nano samples. The utilization of nanostructured standards from GATTAquant GmbH offered the opportunity to test the super-resolution capability of Hamamatsu's leading camera technologies in a quantitative and reproducible way.

2. Introduction

In nature nearly all biomolecules are smaller than 200 nm. As a consequence, the finest structures of fluorescently labeled cells and their molecular components are hidden under the intensity peak from a single point source of light (point-spread function – PSF), which is emitted by a nanoscaled fluorophore. To overcome this barrier, super-resolution microscopy makes use of the changing states of fluorescence markers and measures the shape of the blinking PSF¹. In general there are two main techniques to achieve a bright ON or dark OFF state of fluorophores, either by deterministic photoswitching in space or by stochastically switching single molecule fluorescence ON and OFF in space and time. Prominent methods of the first technique involves ground state depletion (GSD) microscopy², reversible saturable optical fluorescence transition (RESOLFT) microscopy³, linear or saturated structured illumination microscopy^{4, 5} ((S)SIM) or stimulated emission depletion (STED) microscopy⁶. In the field of stochastic imaging (direct) stochastic optical reconstruction microscopy^{7, 8} ((d)STORM), (fluorescence) photo-activation localization microscopy^{9, 10} ((f)PALM), or (DNA-based) point accumulation for imaging in nano-scale topography¹¹ ((DNA-)PAINT) are known to be commonly used.

Nevertheless, whichever technique is applied, samples with standardized dimensions are missing. Recently founded GATTAquant GmbH utilizes state-of-the-art innovations in the field of DNA nanotechnology to fabricate probes for fast, easy and precise quantification of super-resolution systems^{12, 13}. The samples allow the quantification of the resolution of the microscope with a precision of a few nanometers. This is possible by using special nanoconstructs, so called 'DNA origami structures'¹⁴⁻¹⁶, as a breadboard for placing single dye molecules in an exactly defined pattern. This technique allows the placement of fluorophores in preassigned distances, subsequently serving as a ruler on the nanoscale. To study the capabilities of different cameras we focused on nanorulers using DNA-PAINT as SMSN technique (GATTA-PAINT 80R nanoruler). DNA-PAINT is based on the transient binding of fluorophore-labeled "imager" strands to complementary target positions on the nanoruler, enabling a stochastic blinking and subsequently allowing for the reconstruction of a super-resolved image¹⁷.

Besides the blinking technique itself and the optical instrument, which is necessary to perform super-resolution imaging, the camera is a key component. The sensor records the PSF, which is used to reconstruct the super-resolved image. Currently there are two leading camera technologies on the market, which are suitable for super-resolution imaging. In general, both offer a very low readout noise characteristic. The widespread electron multiplying charge coupled device (EM-CCD) cameras multiply the number of electrons on-chip before digitalization. New scientific complementary metal oxide semiconductor (sCMOS) cameras show comparable low-light sensitivities. In general, they are governed by an order of magnitude higher read noise (~1 e⁻) but do not suffer from electron multiplication noise compared to EM-CCDs.

The goal of this white paper is to envision the capability of Hamamatsu's cameras for super-resolution imaging using both EM-CCD and sCMOS technologies with the help of GATTAquant's standardized nanorulers.

3. Imaging technologies

Currently, there are two leading technologies in the field of ultra-low light camera detectors. Super-resolution imaging is clearly considered for ultra-low light applications since typical light levels are less than 1000 photons per pixel per frame. On the one hand there is the Electron Multiplying Charge Coupled Device (EMCCD) sensor which multiplies the photoelectrons in an electron multiplying register on the chip and on the other hand the scientific grade Complementary Metal Oxide Semiconductor (sCMOS) sensor which amplifies the photoelectrons on the pixel directly. Typically, these different signal processes introduce different readout noise levels and characteristics^{20, 21}. The electron multiplication in EMCCD enables the detection of weak light and lowers the readout noise to less than 1e⁻ (rms) but introduces additional noise (excess noise) which lowers the superior quantum efficiency of more than 90 %

Application Note

by a factor of 2. In contrast sCMOS cameras do not suffer from excess noise but show a higher readout noise of $1.4e^-$ (rms). With the help of the following equation the signal to noise ratio can be calculated theoretically

$$SNR = \frac{QE S}{\sqrt{F_n^2 QE (S + I_b) + (N_r/M)}}$$

In the equation QE is the quantum efficiency which is the ratio of incident photons to converted electrons. For the sCMOS camera the peak quantum efficiency is 72 % (at 560 nm) and for the EM-CCD 92 % (at 560 nm). Further, S is the digital signal value in analogue digital units (ADU). I_b is the signal intensity of the background in the experiments. N_r is the readout noise and is a statistical expression of the variability within the electronics that convert the charge of the photoelectrons in each pixel to a digital number. EM gain occurs in a voltage dependent, stepwise manner and the total amount is a combination of the voltage applied and number of steps in the EM register. EM gain has a statistical distribution and an associated variance, which is accounted for by F_n . At typical EMCCD gains up to 1200 $F_n = \approx 1.4$. Since CCD and CMOS do not have EM gain $F_n = 1$ in these cameras. Please note that in this calculation the dark current is neglected because exposure times in localization experiments are typically less than 1 s.

In Figure 1 the signal to noise ratio in absolute values versus input signal photons in number of photons per pixel is plotted. Values are taken from the data sheets of the cameras. The blue line corresponds to the sCMOS camera and the green line to the EM-CCD camera. Additionally the effect of excess noise in EM-CCD cameras is plotted and expressed by the purple line. As sCMOS technology has a six times smaller pixel area, the corrected plot for sCMOS is also shown and denoted as the red line. The graph suggests small advantages for sCMOS technology in terms of sensitivity of more than 10

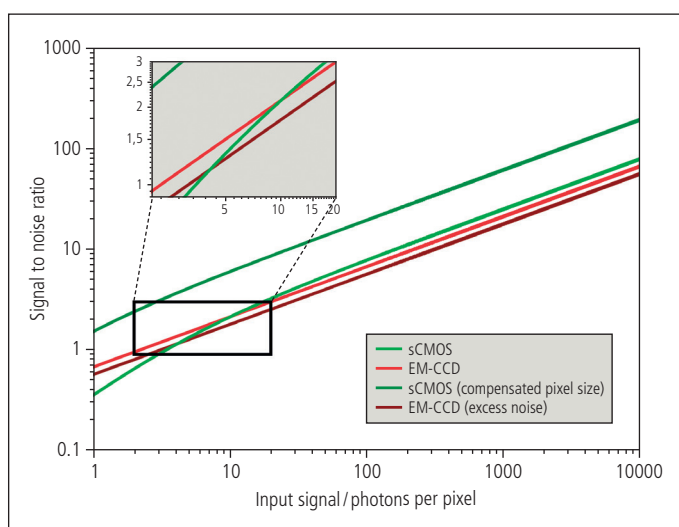


Figure 1: Theoretical Signal to Noise Ratios for EM-CCD (red) and sCMOS (green) in dependency of input photons per individual pixel at 688 nm. The dark red line is the excess noise corrected SNR-plot for the EM-CCD and the dark green line compensates the different pixel sizes of the two sensors.

photons per individual pixel (intersection of blue and green line). If excess noise is accounted for with the EM-CCD, this intersection shifts to 4 photons per individual pixel. However, the corrected pixel sizes for the sCMOS camera reveals a 30 % better SNR.

In some super resolution applications the acquisition speed may be another interesting sensor parameter that makes your application demanding. The EM-CCD camera allows 70 fps at full resolution whereas the rolling shutter in the sCMOS camera allows for an operation at 100 fps at full resolution.

4. Materials and methods

Super-resolution standards (GATTA-PAINT 80R nanoruler) were provided as ready-to-use slides from GATTAquant GmbH, Braunschweig, Germany.

High sensitivity cameras (ImagEM X2 and ORCA-Flash4.0 V2) were provided by Hamamatsu Photonics Deutschland GmbH, Herrsching, Germany.

Super-resolution imaging was performed on a custom-built total internal reflection fluorescence (TIRF) microscope, based on an inverted microscope body (IX71, Olympus). For excitation, a 150 mW, 644 nm diode laser was used (iBeam smart, Toptica Photonics) which was spectrally filtered using a clean-up filter (Brightline HC 650/13, Semrock) and coupled into the microscope with a beamsplitter (zt 647 rdc, Chroma). The laser beam was focused to the backfocal plane of an oil-immersion objective (100x, NA = 1.4, UPlanSApo, Olympus) and aligned for TIRF illumination. In addition, a 1.6x optical magnification was applied resulting in an effective pixel size of 100 nm (EM-CCD) or 40.6 nm (sCMOS). The fluorescence light was spectrally filtered by an emission filter (ET 700/75, Chroma). For imaging, an electron multiplying charge coupled device

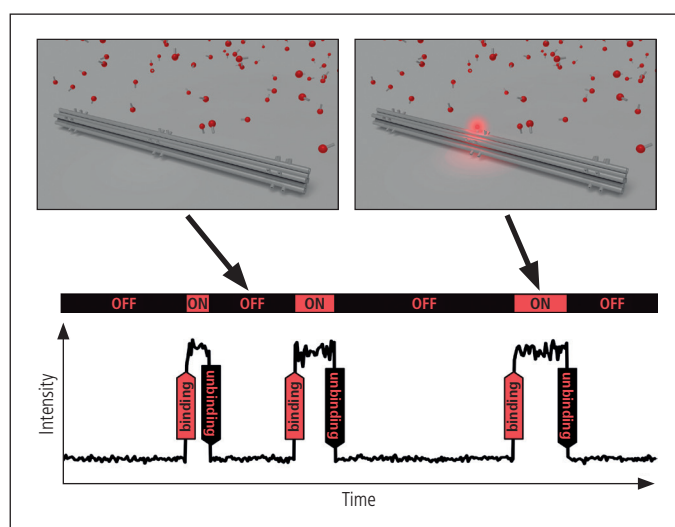


Figure 2: Illustration of the DNA-PAINT imaging technique: The transient binding and unbinding of fluorescently labeled oligonucleotides to specifically designed binding sites, mimics a signal of blinking dye molecules which can be processed in the same way as standard localization based SR microscopy.

Application Note

(EM-CCD, Imagem X2, Hamamatsu) or a scientific complementary metal oxide semiconductor (sCMOS, ORCA-Flash4.0, Hamamatsu) camera was used. To minimize setup and sample drift, the microscope was mounted on an actively stabilized optical table (TS-300, JRS Scientific Instruments). Additionally, the objective was mounted via a nosepiece (IX2-NPS, Olympus).

Typical acquisition parameters were: laser power: $\sim 9 \text{ kW/cm}^2$, integration time: 30 ms, number of frames: 10000, EM gain (for EM-CCD camera): 150. Acquisition was controlled by open source microscopy software Micro-Manager, followed by analysis using custom-built spot finding and 2D-Gaussian fitting algorithms based on MATLAB and LabVIEW. Reconstructed images with resolved nanorulers were finally analyzed using the GATTAAnalysis software from GATTAquant GmbH.

5. Results and discussion

The GATTA-PAINT 80R nanorulers are straight rods based on DNA origami structures, featuring three marks for DNA-PAINT imaging designed with a distance of 80 nm between two adjacent marks (and consequently 160 nm between the two exterior marks). The fluorescence signal is based on the transient binding of ATTO 655 labeled imager oligonucleotides to the complementary target marks on the nanoruler (Figure 2). The data presented originates from the identical probe, whereas the cameras were exchanged during this study.

For both camera types – the EM-CCD and the sCMOS – hundreds of nanorulers could be resolved, confirming the qualitative capability for super-resolution imaging and subsequent image reconstruction. The reconstructed image, given as a 2D heat map of the single events, clearly shows the three in-line marks of the nanoruler (Figure 3a and d). Using the GATTAAnalysis software both the distances between adjacent marks and the full width at half maximum (FWHM) of every individual mark is determined for each ruler, respectively. The results are binned in a histogram and fitted accordingly with a Gaussian. The EM-CCD camera shows an average distance of $(77 \pm 14) \text{ nm}$ for the GATTA-PAINT 80R nanoruler (Figure 3b) with a FWHM of $(25 \pm 6) \text{ nm}$ (Figure 3c). Using the same acquisition parameters for the sCMOS camera, the distance values of $(79 \pm 18) \text{ nm}$ tend to be very similar in comparison to the EM-CCD camera (Figure 3e), nevertheless the FWHM is clearly shifted to $(19 \pm 8) \text{ nm}$, resulting in an improved FWHM by 24 % (Figure 3f).

In the following the intensity signals of the blinking events are identified in detail for both the EM-CCD and sCMOS. Therefore, 10 intensity levels from the blinking spots from 10 different frames are measured. The EM-CCD showed average intensity values of $(29,098 \pm 8,590) \text{ ADU}$ and the sCMOS $(768 \pm 266) \text{ ADU}$. Both camera sensors allow 16 bit ADU values so that the EM-CCD is saturated by 44 % and the sCMOS to only 1.2 % on average. However to calculate the signal to noise ratio the background signal also has to be taken into account. To identify the average background signals the mean value of a square is measured (see Figure 4). The EM-CCD has background intensities

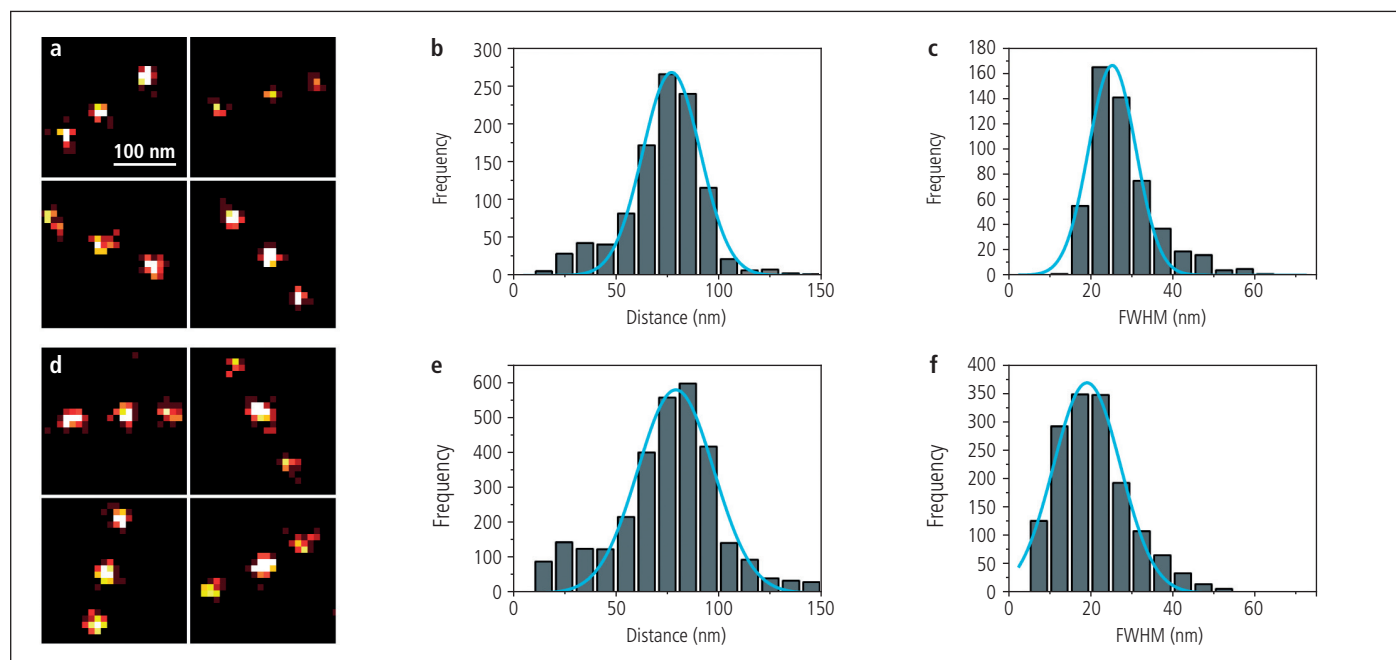


Figure 3: a) DNA-PAINT images of GATTA-PAINT 80R nanorulers acquired with an EM-CCD camera. b) Gained distance histogram showing an average distance of $(77 \pm 14) \text{ nm}$. c) Gained histogram of the individual mark FWHMs showing an average FWHM of $(25 \pm 6) \text{ nm}$. d) DNA-PAINT images of GATTA-PAINT 80R nanorulers acquired with an sCMOS camera. e) Gained distance histogram showing an average distance of $(79 \pm 18) \text{ nm}$. f) Gained histogram of the individual mark FWHMs showing an average FWHM of $(19 \pm 8) \text{ nm}$.

Application Note

of $(15,224 \pm 564)$ ADU and the sCMOS (282 ± 21) ADU. Now these values can be used to calculate the signal to noise ratios as previously explained (see equation 1). The EM-CCD shows a SNR of 93 per pixel and the sCMOS 20 per pixel. Considering the six times smaller pixel area ($256 \mu\text{m}^2 / 42.25 \mu\text{m}^2 = 6$) of the sCMOS this value increases to 120. In other words the sCMOS sensor has an improved SNR of 30 %. This fact validates the theoretical SNR consideration discussed before (see Imaging Technologies).

Nevertheless the intensities are highly sufficient for threshold-based spot finding and subsequent 2D Gaussian fitting. The calculated distance values of the reconstructed nanorulers only slightly deviate for each camera type. Further they strongly agree with the designed distance of 80 nm within the given standard error. The FWHM for the EM-CCD is found to be around 25 nm, a value comparable to previous DNA-PAINT measurements¹⁷⁻¹⁹. Nevertheless, our finding that the FWHM for the sCMOS is around 19 nm opens the potential use of these camera types for single molecule measurements.

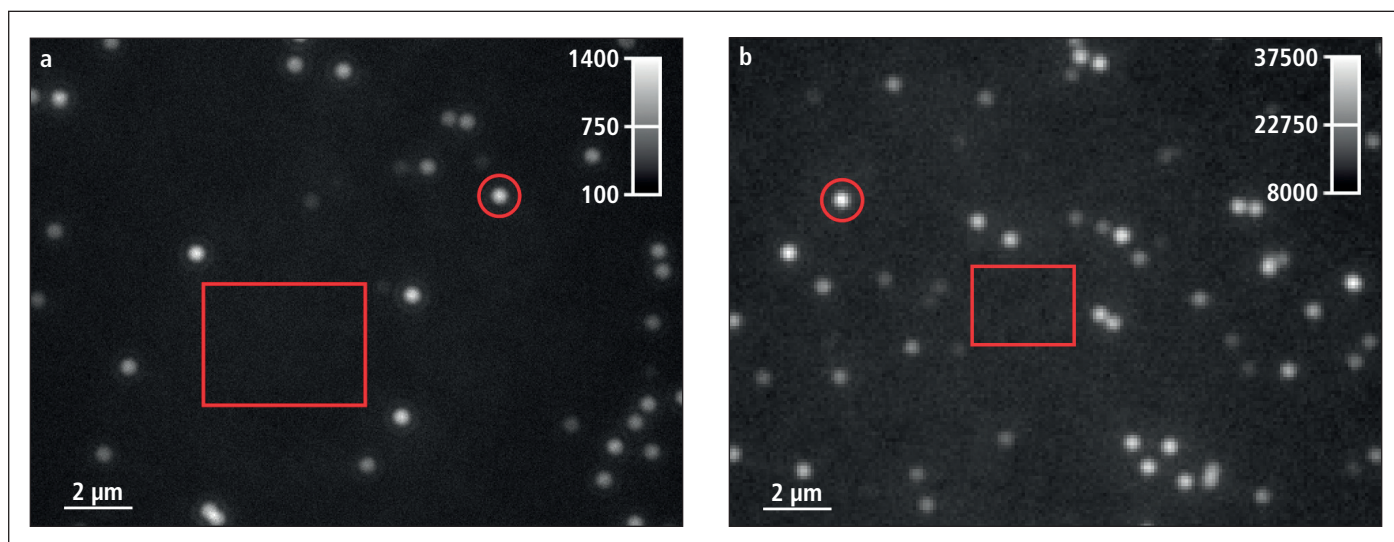


Figure 4: a) sCMOS raw image (480 x 360 pxls) b) EM-CCD raw image (192 x 144 pxls). The images are 8bit LUT corrected. A red square identifies the area where the background intensity was identified in the SNR calculation. The red circle measures a PSF of a fluorophore. The color scales indicate the intensity values in ADU.

6. Conclusions

The utilization of GATTAquant's standardized nanostructures for super-resolution microscopy offers a variety of advantages compared to previous test samples like microtubules or fluorescent beads. It is the first time that a large amount of identical patterns, with defined distances, is available and these nanorulers allow for the parallel analysis and statistical validation of the resolution of the set-up. In addition, their fluorescent properties are – due to the selected type and number of dyes – comparable to real samples, for instance mimicking classically stained cell samples in a more comparable way to setup parameters and settings.

Now, the utilization of these standard probes enables the verification of the performance of different camera types under uniform (or stable) conditions. The statistical data evaluation allows a direct comparison of Hamamatsu's EM-CCD and sCMOS cameras and confirms their benefit for super-resolution imaging.

The SNR measurement showed small advantages for sCMOS technology. Recently, Hamamatsu launched a new sCMOS camera with 10 % increase of quantum efficiency over the visible spectra. This makes sCMOS technology even more suitable for super-resolution imaging.

Key words

DNA-PAINT, Standardized Super Resolution, Ultra Low Light Camera, Nano-ruler, sCMOS, EM-CCD

Authors

Dr. Benjamin Eggart, Application Engineer
+49 (8152) 375 205, beggart@hamamatsu.de
Hamamatsu Photonics Deutschland GmbH
<http://www.hamamatsu.de>

Dr. Max Boy Scheible, Research and Development
+49 (531) 391 5349, scheible@gattaquant.com
GATTAquant GmbH
<http://www.gattaquant.com/>

Dr. Carsten Forthmann
+49 (531) 391 5349, forthmann@gattaquant.com
GATTAquant GmbH
<http://www.gattaquant.com/>

Application Note

References

1. Hell, S. W., Far-field optical nanoscopy. In *Science*, 2007; Vol. 316, p 1153.
2. Hell, S. W.; Kroug, M., Ground-state-depletion fluorescence microscopy: A concept for breaking the diffraction resolution limit. In *Applied Physics B*, Springer: 1995; Vol. 60, pp 495-497.
3. Hofmann, M.; Eggeling, C.; Jakobs, S.; Hell, S. W., Breaking the diffraction barrier in fluorescence microscopy at low light intensities by using reversibly photoswitchable proteins. In *Proc Natl Acad Sci USA*, 2005; Vol. 102, pp 17565-17569.
4. Gustafsson, M. G. L., Surpassing the lateral resolution limit by a factor of two using structured illumination microscopy. In *Journal of Microscopy*, 2000; Vol. 198, pp 82-87.
5. Gustafsson, M., Nonlinear structured-illumination microscopy: Wide-field fluorescence imaging with theoretically unlimited resolution. In *Proceedings of the National Academy of ...*, 2005.
6. Hell, S. W.; Wichmann, J., Breaking the diffraction resolution limit by stimulated emission: stimulated-emission-depletion fluorescence microscopy. In *Opt Lett*, Optical Society of America: 1994; Vol. 19, pp 780-782.
7. Rust, M. J.; Bates, M.; Zhuang, X., Sub-diffraction-limit imaging by stochastic optical reconstruction microscopy (STORM). In *Nat Meth*, 2006; Vol. 3, pp 793-795.
8. Heilemann, M.; van de Linde, S.; Schüttel, M.; Kasper, R.; Seefeldt, B.; Mukherjee, A.; Tinnefeld, P.; Sauer, M., Subdiffraction-Resolution Fluorescence Imaging with Conventional Fluorescent Probes. In *Angew Chem Int Ed Engl*, 2008; Vol. 47, pp 6172-6176.
9. Betzig, E.; Patterson, G. H.; Sougrat, R.; Lindwasser, O. W.; Olenych, S.; Bonifacino, J. S.; Davidson, M. W.; Lippincott-Schwartz, J.; Hess, H. F., Imaging intracellular fluorescent proteins at nanometer resolution. In *Science*, 2006; Vol. 313, pp 1642-1645.
10. Hess, S. T.; Girirajan, T. P. K.; Mason, M. D., Ultra-high resolution imaging by fluorescence photoactivation localization microscopy. In *Biophys J*, 2006; Vol. 91, pp 4258-4272.
11. Sharonov, A.; Hochstrasser, R., Wide-field subdiffraction imaging by accumulated binding of diffusing probes. In *Proc Natl Acad Sci USA*, 2006; Vol. 103, p 18911.
12. Schmied, J. J.; Gietl, A.; Holzmeister, P.; Forthmann, C.; Steinhauer, C.; Dammeyer, T.; Tinnefeld, P., Fluorescence and super-resolution standards based on DNA origami. In *Nat Meth*, 2012; Vol. 9, pp 1133-1134.
13. Schmied, J. J.; Raab, M.; Forthmann, C.; Pibiri, E.; Wünsch, B.; Dammeyer, T.; Tinnefeld, P., DNA origami-based standards for quantitative fluorescence microscopy. In *Nat Protoc*, 2014; Vol. 9, pp 1367-1391.
14. Rothmund, P. W. K., Folding DNA to create nanoscale shapes and patterns. In *Nature*, 2006; Vol. 440, pp 297-302.
15. Douglas, S. M.; Dietz, H.; Liedl, T.; Högberg, B.; Graf, F.; Shih, W. M., Self-assembly of DNA into nanoscale three-dimensional shapes. In *Nature*, 2009; Vol. 459, pp 414-418.
16. Dietz, H.; Douglas, S. M.; Shih, W. M., Folding DNA into twisted and curved nanoscale shapes. In *Science*, 2009; Vol. 325, pp 725-730.
17. Jungmann, R.; Steinhauer, C.; Scheible, M. B.; Kuzyk, A.; Tinnefeld, P.; Simmel, F. C., Single-molecule kinetics and super-resolution microscopy by fluorescence imaging of transient binding on DNA origami. In *Nano Lett*, 2010; Vol. 10, pp 4756-4761.
18. Lin, C.; Jungmann, R.; Leifer, A. M.; Li, C.; Levner, D.; Church, G. M.; Shih, W. M.; Yin, P., Submicrometre geometrically encoded fluorescent barcodes self-assembled from DNA. In *Nat Chem*, 2012; Vol. 4, pp 832-839.
19. Scheible, M. B.; Pardatscher, G.; Kuzyk, A.; Simmel, F. C., Single molecule characterization of DNA binding and strand displacement reactions on lithographic DNA origami microarrays. In *Nano Lett*, 2014; Vol. 14, pp 1627-1633.
20. Hernandez-Palacios, J., and L. L. Randeberg. "Intercomparison of EMCCD- and sCMOS-based imaging spectrometers for biomedical applications in low-light conditions." SPIE BiOS. International Society for Optics and Photonics, 2012.
21. Long, Fan, Shaoqun Zeng, and Zhen-Li Huang. "Localization-based super-resolution microscopy with an sCMOS camera Part II: Experimental methodology for comparing sCMOS with EMCCD cameras." *Optics express* 20.16 (2012): 17741-17759.